Journal of Physics D: Applied Physics

PAPER

Y_2O_3-based memristive crossbar array for synaptic learning

IOP Publishing Journal of Physics D: Applied Physics
J. Phys. D: Appl. Phys. 55 (2022) 205103 (8pp) https://doi.org/10.1088/1361-6463/ac485b

Y_2O_3-based memristive crossbar array for synaptic learning

Mohit Kumar Gautam[1], Sanjay Kumar[1] and Shaibal Mukherjee[1,2,*]

[1] Hybrid Nanodevice Research Group (HNRG), Department of Electrical Engineering, Indian Institute of Technology Indore, Simrol, Madhya Pradesh 453552, India
[2] Centre for Advanced Electronics (CAE), Indian Institute of Technology Indore, Simrol, Madhya Pradesh 453552, India

E-mail: shaibal@iiti.ac.in

Received 5 December 2021, revised 23 December 2021
Accepted for publication 5 January 2022
Published 17 February 2022

Abstract

Here, we report the fabrication of an Y_2O_3-based memristive crossbar array along with an analytical model to evaluate the performance of the memristive array system to understand the forgetting and retention behavior in the neuromorphic computation. The developed analytical model is able to simulate the highly dense memristive crossbar array-based neural network of biological synapses. These biological synapses control the communication efficiency between neurons and can implement the learning capability of the neurons. During electrical stimulation of the memristive devices, the memory transition is exhibited along with the number of applied voltage pulses, which is analogous to the real human brain functionality. Further, to obtain the forgetting and retention behavior of the memristive devices, a modified window function equation is proposed by incorporating two novel internal state variables in the form of forgetting rate and retention. The obtained results confirm that the effect of variation in electrical stimuli on forgetting and retention is similar to that of the biological brain. Therefore, the developed analytical memristive model can further be utilized in the memristive system to develop real-world applications in neuromorphic domains.

Keywords: Y_2O_3, crossbar, memristive devices, synapses

(Some figures may appear in colour only in the online journal)

1. Introduction

Artificial neural networks are inspired by the remarkable efficacy of biological systems, and can be practically realized by utilizing two-terminal memristive devices [1]. Further, the emulation of the synapse is a promising step toward the enhancement of efficiency of artificial neural networks [2]. The synapse is one of the fundamental cellular units of the biological neural unit [3]. More specifically, in the biological nervous system, neurons are interconnected with one another through synapses, and information gets transferred from pre-synaptic to post-synaptic neurons via synapses [3, 4]. During this transfer, the synaptic weight of the synapse, which is analogous to the memristive device conductance, can be modulated under the application of electrical stimuli [5]. The synaptic weight is strengthened under the application of positive electrical stimuli, while in the case of negative electrical stimuli, the synaptic weight is debilitated [4].

In the neuromorphic computation, the strengthened and debilitated processes are termed as the potentiation and depression mechanism, respectively [4, 5]. The synaptic weight of the memristive device can be dynamically varied according to the use of electrical pulse excitations [6, 7]. Synaptic plasticity is the fundamental functionality of the biological brain to change and receive new information, and plays a vital role in the learning and forgetting process in the human brain [8].

Neuromorphic computation requires ultralow power, high-density networks, remarkable efficiency and complementary metal oxide semiconductor-compatible devices and systems [7, 9]. A memristive system fulfilling all these requirements

* Author to whom any correspondence should be addressed.

would make it a highly suitable candidate for neuromorphic computation [5], synaptic functionality [10] and data storage applications [11]. Besides these, memristive systems are able to show various synaptic functionalities, such as non-linear transmission characteristics [12], spike-rate-dependent plasticity [2], spike-timing-dependent plasticity [2], long-term potentiation (LTP) [13], short-term plasticity (STP) [13], learning behavior [14] and forgetting behavior [14], and short-term memory (STM) [15] and long-term memory (LTM) [15] behaviors of the real biological synapse.

Recently, our research group successfully developed Y_2O_3-based [16, 17] memristive devices for neuromorphic computation, in which an Y_2O_3-based resistive switching layer (SL) is grown by utilizing a dual ion beam sputtering (DIBS) system. The DIBS system offers multiple advantages, such as high-quality thin films with better compositional stoichiometry and controllability, small surface roughness and good adhesion of the deposited thin film to the substrate [16, 17] as compared to other conventional physical vapor deposition techniques.

In this article, a detailed fabrication process for a memristive crossbar array along with electrical and surface morphological characterization are discussed. Furthermore, a non-linear analytical model has also been proposed to investigate the performance of the developed memristive crossbar array by modeling the resistive switching response of the system. The analytical model is further extended for synaptic plasticity in terms of LTP and STP, forgetting rate and retention behaviors with STM and LTM functionality. The proposed model is an enhanced version of our previously reported model [18] to analyze the forgetting rate and retention behaviors with STM and LTM functionality. The discussed model fulfills all the essential conditions as detailed by Prodromakis *et al* [19].

2. Experimental

Figure 1 describes the detailed fabrication process to realize the Y_2O_3-based memristive crossbar array using the DIBS system [16, 17]. During the fabrication process, metal shadow masks are used to pattern the bottom electrode (BE), switching layer (SL) and top electrode (TE) of the crossbar array. For the (4 × 4) crossbar array fabrication, a 3 inch cleaned Si (100) substrate is utilized, as shown in figure 1(a). Further, an Ar^+ plasma etching process is performed for 15 min by the secondary ion assist source in the DIBS system to remove the native ultrathin SiO_2 layer on top of Si [16]. After the removal of native oxide, 150 nm thick polycrystalline Y_2O_3 is grown over the Si substrate as an insulating layer [17], as shown in figure 1(b) at 100 °C in a pure Ar (5 sccm) environment in the assist ion source of the DIBS system. The deposited insulating layer has a remarkable surface morphology and smoothness due to the similar lattice constants of Si ($2a_{\mathrm{Si}} = 10.86$ Å) and Y_2O_3 ($a_{\mathrm{Y2O3}} = 10.60$ Å), as reported elsewhere [20, 21].

Furthermore, a low resistive (5.3×10^{-4} Ω·cm) [22] Ga-doped ZnO (GZO) with 100 nm thickness is grown over the insulating Y_2O_3 layer at 100 °C in a pure Ar (5 sccm) environment in the assist ion source. The deposited GZO acts as the BE and is patterned via a shadow mask with a width of 800 μm, as shown in figure 1(c). Subsequently, a 50 nm amorphous Y_2O_3 layer is deposited as a resistive SL, as shown in figure 1(d). The SL is deposited at 300 °C at a fixed ratio of Ar to O_2 gas flow of 2:3 in the assist ion source of the DIBS system [19]. At the end, a 70 nm Al TE is deposited via a direct-current (DC) magnetron sputtering system, as presented in figure 1(e). The line width of the TE shadow mask is 300 μm. Figures 1(f) and (g) show a schematic and digital camera photograph of the finally fabricated 4 × 4 crossbar memristive array. To investigate the resistive switching performance of the fabricated crossbar array architecture, a semiconductor parameter analyzer (SCS-4200A) system is utilized. Further, optical microscopy is performed to visualize the realistic view of the fabricated crossbar array, and field emission scanning electron microscopy (FESEM, Carl Zeiss) is used to assist in the surface morphological analysis.

Subsequent to the fabrication and performance measurement of the memristive device, it is essential to analyze the performance to understand the underlying physics, and analytical modeling is essential. Previously, several analytical [15, 23–25] and circuit models [4] have been reported; however, none of the reported models have been validated with respect to the memristive crossbar array response. Some of the earlier reported models [15, 24, 25] have not been validated with the experimental results. Here, a memristive crossbar analytical model with experimental validation has been formulated to emulate the various memristive device properties, as discussed in a detailed manner in section 4.

3. Analytical model

Equation (1) describes the current–voltage (I–V) relationship that governs the switching characteristics of the Y_2O_3-based crossbar [18]:

$$I(t) = \left\{ \begin{array}{l} b_1 w^{a_1}\left(e^{\alpha_1 V_{\mathrm{i}}(t)} - 1\right) + \chi\left(e^{\gamma V_{\mathrm{i}}(t)} - 1\right), V_{\mathrm{i}}(t) \geq 0 \\ b_2 w^{a_2}\left(e^{\alpha_2 V_{\mathrm{i}}(t)} - 1\right) + \chi\left(e^{\gamma V_{\mathrm{i}}(t)} - 1\right), V_{\mathrm{i}}(t) < 0 \end{array} \right\}. \tag{1}$$

Here, the first term described on the right-hand side of (1) is associated with the flux-controlled memristive behavior due to the interfacial switching mechanism and is not reported in previously reported models [23–25]. Here, the parameters a_1 and a_2 determine the degrees of influence of the state variable on the device current for positive and negative polarities of the applied bias voltage, respectively. b_1 and b_2 are designated as the experimental fitting parameters, which describe the conductivity slope in resistive switching characteristics as shown in figure 2(c). w is the internal state variable, and α_1 and α_2 are the pinched hysteresis loop area controlling parameters. The second term on the right-hand side of (1) stands for the ideal diode behavior in resistive switching characteristics and plays a key role when the internal state variable (w) approaches zero, and parameters χ and γ denote the net electronic barrier of the memristive device. $V_{\mathrm{i}}(t)$ is the applied input bias voltage.

A piecewise window function $f(w)$ is utilized as described in (2) [18]. The window function ensures that w is restricted between 0 and 1. In the analytical modeling, a constant value

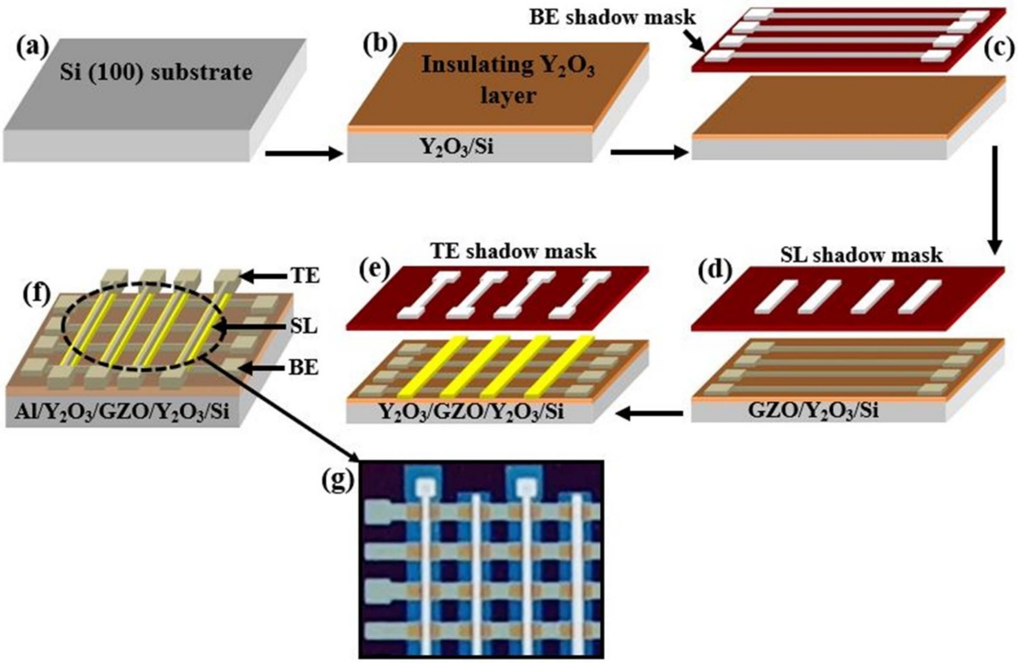

Figure 1. Schematic diagram of (a) cleaned Si substrate, (b) deposition of insulating Y_2O_3 layer on top of Si, (c) BE deposition via DIBS system, (d) SL deposition via DIBS system, (e) TE deposition via DC magnetron sputtering. (f) A schematic and (g) digital camera photograph of the finally fabricated 4 × 4 crossbar array architecture.

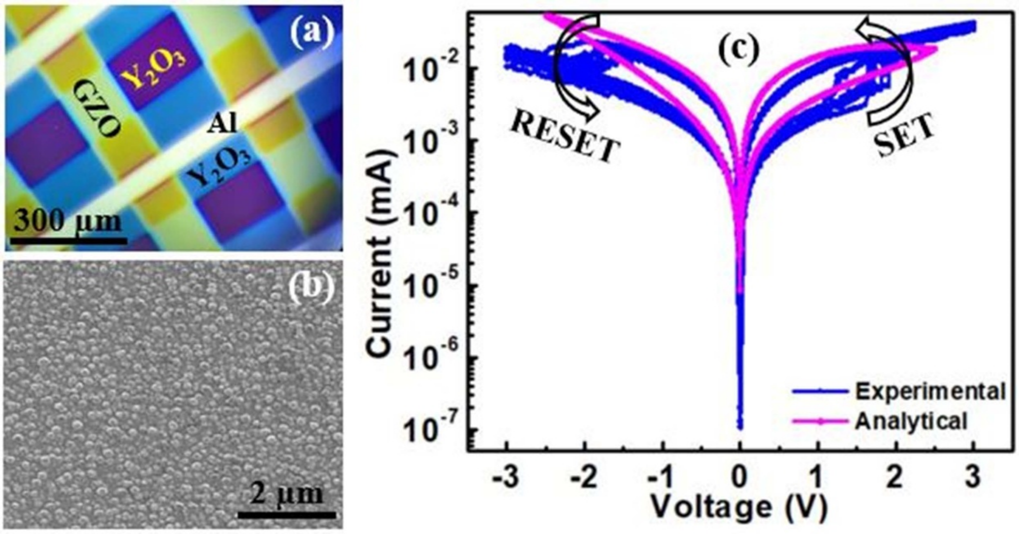

Figure 2. (a) Magnified optical microscopy images of developed memristive crossbar array architecture, (b) FESEM images of top surface of Y_2O_3 SL, (c) resistive switching response of the fabricated memristive crossbar array fitted with the analytical model.

of $p = 2$ is used. The value of the parameter p helps one to limit the value of $f(w)$ ε {0, 1}. However, for $p > 10$, the upper limit of $f(w)$ is beyond 1, and thus violates the essential conditions for $f(w)$, which is defined between 0 and 1, as reported by Kumar *et al* [16] and Prodromakis *et al* [19]:

$$f(w) = \log \left\{ \begin{array}{l} (1+w)^{\mathrm{P}}, 0 \leq w \leq 0.1 \\ (1.1)^{\mathrm{P}}, 0.1 < w \leq 0.9 \\ (2-w)^{\mathrm{P}}, 0.9 < w \leq 1 \end{array} \right\}. \quad (2)$$

Equation (3) describes the time derivative of the internal state variable $(w(t))$ [18] and is further modified by incorporating two important parameters, namely *viz* the forgetting rate (τ) and retention (t_r) to emulate the retention and forgetting behavior of the memristive crossbar array. The time derivative of the $(w(t))$ is dependent on the nature of the input voltage, window function and forgetting and retention terms of the memristive crossbar model. However, the previously reported model [15] has not been experimentally validated for the switching response of the memristive crossbar array:

Table 1. Modeling parameter values and their physical interpretation.

Parameters	Values/range	Physical interpretation
b_1	1.59×10^{-3}	Experimental fitting parameters
b_2	-6.2×10^{-4}	Experimental fitting parameters
a_1	1.2	Degrees of influence of the state variable under positive bias
a_2	0.3	Degrees of influence of the state variable under negative bias
α_1	0.60	Hysteresis loop area controlling parameters under positive bias
α_2	−0.68	Hysteresis loop area controlling parameters under negative bias
χ	1×10^{-11}	Magnitude of ideal diode behavior
γ	1	Diode parameters such as thermal voltage and ideality factor
A	5×10^{-4}	Control the effect of the window function
m	5	Control the effect of input on the state variable
p	$0 < p \leqslant 10$	Bounding parameter for window function between 0 and 1
τ	0.15	Forgetting rate
t_r	0.1	Retention; t_r ε [0,1]
σ	1×10^{-6}	Corresponding parameters for t_r and τ
θ	1×10^{-7}	Corresponding parameters for t_r and τ
η_1	4	Interface effect with positive and negative voltage and independent of w
η_2	2	Interface effect with positive and negative voltage with positive-valued parameters and determined by the SL material properties and independent of w

$$\frac{dw}{dt} = \left\{ A \times V_{\mathrm{i}}^{\mathrm{m}}(t) \times f(w) - \left(\frac{w - t_{\mathrm{r}}}{\tau} \right) \right\}. \tag{3}$$

where A and m are the parameters that define the dependence of the state variable on the input voltage, and m ensures that the opposite polarity of the applied voltage leads to an opposite change in the rate of change of the state variable. The last term on the right-hand side of (3) is associated with the memory forgetting rate (τ) and retention (t_r) behavior of the memristive device. The voltage derivative of forgetting rate and retention can be defined by (4) and (5), respectively:

$$\frac{d\tau}{dv} = \theta \left(e^{\eta_1 \mathrm{v}} - e^{-\eta_2 \mathrm{v}} \right). \tag{4}$$

$$\frac{dt_{\mathrm{r}}}{dv} = \sigma \left(e^{\eta_1 \mathrm{v}} - e^{-\eta_2 \mathrm{v}} \right) \times f(w) \tag{5}$$

where η_1 expresses the interface effect with positive and negative voltage and is considered as positive-valued fitting parameter, and η_2 represents the material properties, such as activation energy [4]. The value of t_r is limited between 0 and 1, i.e. t_r ε[0, 1], and σ and θ are the corresponding parameters for t_r and τ and are considered as constants during the analytical modeling.

Equations (4) and (5) are used to accurately model the synaptic plasticity; more specifically, the STM and LTM properties. The value of τ denotes the forgetting rate, which is greater than 0 ($\tau > 0$), and θ and σ are always positive-valued parameters to analyze the forgetting rate and the retention behavior of the memristive crossbar array systems. Table 1 presents the physical interpretation and numerical values of all parameters used in the analytical modeling.

4. Results and discussion

Figure 2(a) shows optical microscopy image of the developed memristive crossbar array, which clearly shows that the deposited layers are perfectly aligned to form a crosspoint structure in the array. Figure 2(b) exhibits a continuous Y_2O_3 SL layer with compact grains, which is also described in our earlier report [16].

To analyze the resistive switching response of the fabricated crossbar array, the TE is connected to the positive/negative voltage terminal of the SCS-4200A while the BE is fixed to the ground. To examine the switching response, a triangular voltage waveform is applied to the device with an amplitude of ±3 V and a pulse width of 100 ms, and captures the resistive switching performance of the device as shown in figure 2(c). Further, when a positive voltage (0 to +3 V) is imposed on the TE, the device switches from a high resistance state (HRS) to a low resistance state (LRS) and this process is termed the 'SET' process, as shown in figure 2(c). The detailed switching mechanism of the Y_2O_3-based memristor is described in our previous report [26].

For a negative voltage bias (from 0 to −3 V) applied on TE, the device switches from LRS to HRS [26], and this process is known as the RESET process, as depicted in figure 2(c). Figure 2(c) also reveals that the developed crossbar array shows a consistent resistive switching response in multiple switching cycles, and toggles between HRS and LRS and back without any noticeable change in the SET and RESET voltages. The negligible variation in the SET and RESET voltages signifies that the DIBS system is extremely promising to develop a reliable and stable memristive crossbar array. The analytical model, as discussed above, also captures the resistive switching behavior with an R^2-fitting accuracy of 99.2% with corresponding experimentally obtained data of the fabricated crossbar array. The accuracy of the model

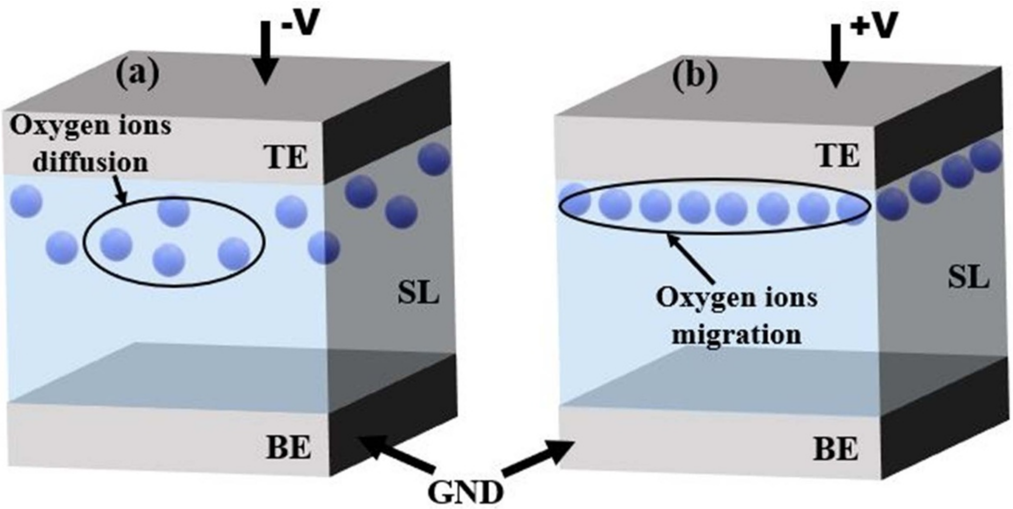

Figure 3. (a) Ion diffusion and (b) ion migration at the memristive device interface.

is comparatively higher than that observed in our previous reports [18, 23], in which ∼98% [18] and ∼96% [23] accuracy levels were reported. Besides that, the presented model has also shown better accuracy as compared to previously reported models [15, 24, 25] in terms of the stable switching response, with a better hysteresis loop area in multiple cycles, as shown in figure 5. The presence of a pinched hysteresis loop in the resistive switching characteristics of the device is a footprint of the memristive system [27], and the pinched hysteresis loop can be collapsed into a single-valued function as described by Chua [28].

It is known that the conductance of memristive systems is dependent on various parameters, such as the input pulse amplitude, pulse time duration and time interval between two consecutive pulses. Here, figure 4(a) analytically shows the variation in the memristive device conductance with respect to the number of pulses, in which ten consecutive voltage pulses with different amplitude and time duration are imposed on the memristive crossbar. It is observed that the pulses with larger voltage amplitude and longer time duration trigger a larger change in the device conductance, while on the other hand, the pulses with smaller amplitude and shorter time duration result in a negligible or no change in the device conductance, which is associated with the device activation state. However, the relentless competition between ion diffusion and ion migration, as shown in figure 3, at the device interface decides the net conductance of the memristive device. The ion diffusion decreases the device conductance while ion migration increases the device conductance [15, 29, 30].

Figure 3(a) shows the ion diffusion process under the application of negative applied voltage at the TE, in which the net concentration of oxygen ions is less at the interface, which affects the interface conduction and further leads to a decrement in the device conductance [31–35]. On the other hand, under the application of applied positive voltage at the TE, the oxygen ion migration process takes place at the interface and the concentration of oxygen ions is higher at the device interface, which leads to an increment in device conductance at the interface [31–35], as shown in figure 3(b). Further, the time duration and interval have a significant impact on the device conductance [36, 37], as depicted in figure 4(b). For this analysis, ten consecutive voltage pulses with the same amplitude and different time duration and interval are applied on the memristive crossbar, and it is observed that the pulses with shorter intervals induce a larger change in the device conductance as compared to pulses with longer time intervals. This is because, in general, the longer time interval leads to ion diffusion, which substantially reduces the device conductance [15]. Similar memory plasticity is experimentally demonstrated by Das *et al* [17] in a DIBS-grown Y_2O_3-based single memristive device. In that work, the memristive device conductance is varied with the number of input pulses, and the impact of the conductance is investigated by the variation of pulse amplitude and duration. The experimental results reported by Das *et al* [17] are analytically verified by Kumar *et al* [18].

Further, the proposed model also captures the change in device current under the application of successive voltage sweeps, as shown in figure 5. Figure 5(a) represents a continuous enhancement of the device current (or conductance) under the application of successive positive voltage sweeps, and this phenomenon is analogous to the potentiation mechanism of memristive systems [4, 5]. On the other hand, for successive negative voltage sweeps, the device current (or conductance) continuously declines, as presented in figure 5(b), which is analogous to the depression mechanism of memristive systems [4, 5].

Figure 6 shows the retention and forgetting rate in the improved diffusion term and it is varied along with the time for which the electric field is applied. The direction of the ion diffusion is determined by the comparative result of the conductance and the retention. When $w > t_r$, the positive electrical field is overlapped, while an overlapping negative electric field is observed when $w < t_r$. In other cases, the ion diffusion mechanism promotes the increment or decrement in the device conductance, i.e. the ion diffusion process has the same direction

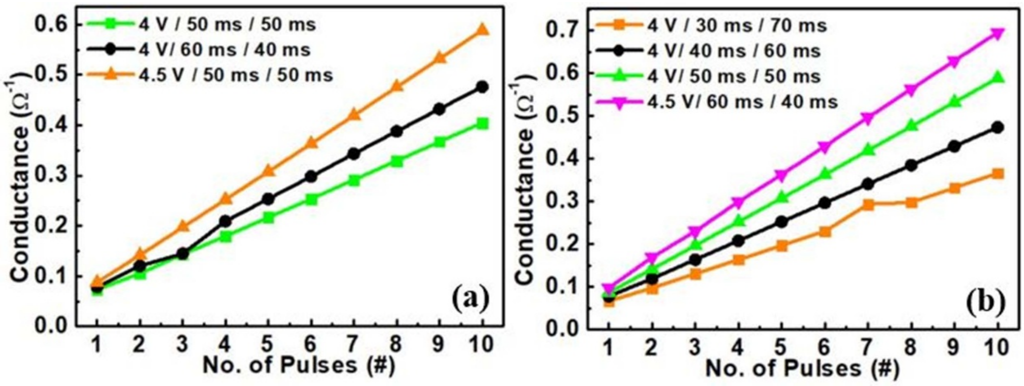

Figure 4. The plasticity of memristive crossbar using (a) pulses with different amplitude and duration, (b) pulses with different interval with constant amplitude. Here, the format of the labels, i.e. 4 V/50 ms/50 ms, shows the pulse amplitude, pulse width and interval between two consecutive pulses, respectively.

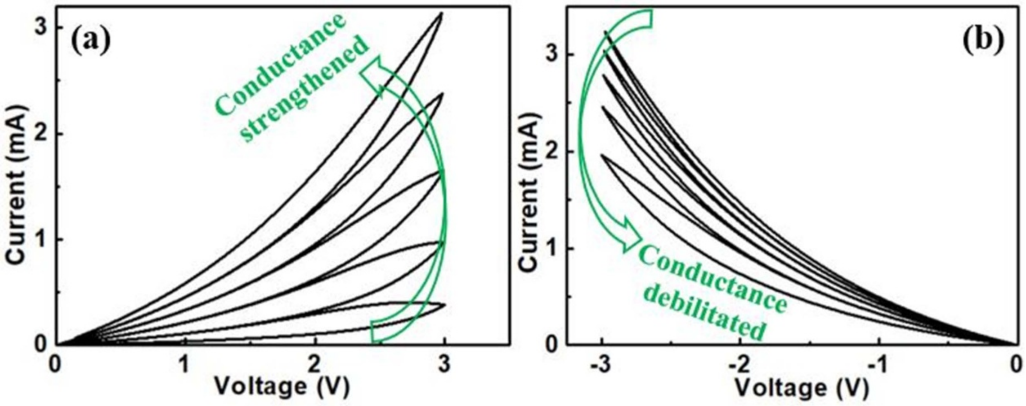

Figure 5. I–V curves of memristive systems under consecutive (a) positive voltage pulses of +3 V and (b) negative voltage pulses of −3 V. The change in device current/conductance is the basis of synaptic plasticity in memristive systems.

as the ion migration [15]. Moreover, the asymmetric variation in the positive and negative electric field, τ and t_r, vary more rapidly under a positive electric field as compared to the case for a negative electric field, as shown in figure 6(a). From figure 6(b), it is clear that the forgetting rate and the retention are improved significantly under the application of repeated electrical stimulation. The forgetting rate increases from 0.15 to 0.26 s along with the increasing input stimuli number. At the same time, as shown in figure 6(b), the retention also increases from 10% to 20.1%, which is comparatively better than the previously reported data [15], 6 and the increment in forgetting rate and retention indicate a clear transition from STM to LTM [15].

Another important behavior of a memristive system is the transition from STM to LTM, which is captured by the proposed analytical model. As shown in figure 7(a), 20 consecutive input pulses of +4 V amplitude and 40% duty cycle are imposed on the memristive device. Under the application of each electrical stimulation, the device conductivity is first increased, followed by a decay due to spontaneous diffusion, as mentioned earlier. However, when the time interval between the successive stimulation is relatively short, in the range of 5–30 ms, an overall increment in the conductance is observed despite the spontaneous decay, as shown in figure 7(a). This phenomenon is caused by the competing process between diffusion and ion migration [15, 29, 30, 36]. Moreover, the stabilization in the switching process and persistence of LTM are evidence of the growth of new synaptic connections and a change in the shape and size of the pulse, adding more pathways for synaptic transmission. LTM fades with time, showing that the synaptic connections revoke with time, but at a much slower speed compared to the decay in STM [36].

Figure 7(b) shows the synaptic plasticity behavior in terms of the potentiation and depression processes of the memristive device [4, 5, 17]. During a positive electrical stimulus, the synaptic weight or the normalized conductance of the memristive device is continuously strengthened, while under a negative electrical stimulus, the synaptic weight is gradually debilitated. Figure 7(b) further displays the re-stimulation process followed by the first stage of the potentiation and depression processes, in which a comparatively smaller number of electrical input stimuli are required to achieve the same stage of memory learning process. This phenomenon is similar to the learning behavior of biological systems, which allows relearning of the elapsed information to be at a much faster rate [17, 36–42].

The extensive benefits of the discussed analytical model are that it is able to emulate the forgetting and retention behavior

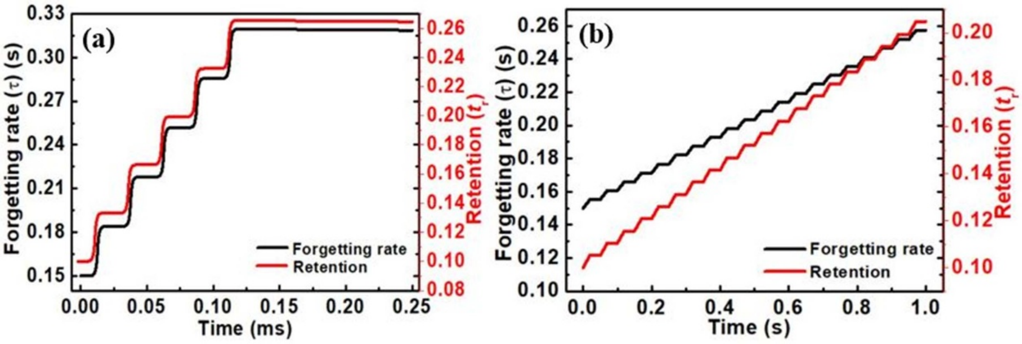

Figure 6. (a) and (b) τ–t and t_r–t curves.

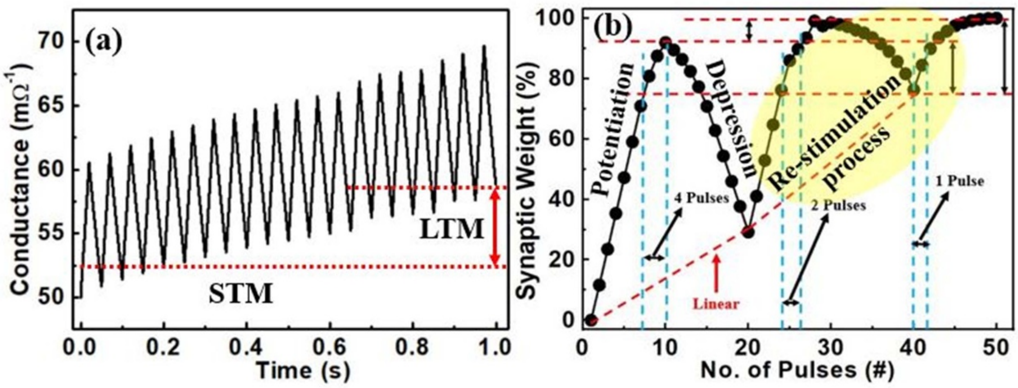

Figure 7. (a) Transition from STM to LTM in which conductance varies along with stimulation pulses, (b) potentiation and depression processes along with restimulation process.

and STM-to-LTM transition precisely, which was not captured by earlier reported models [18, 23, 25]. Further, the proposed model also has the ability to capture the realistic behavior of biological systems, which helps engineers and researchers to analyze the various functionalities of biological systems. Moreover, the developed analytical memristive model is also able to compute the diverse real-time neuromorphic characteristics.

5. Conclusion

Here, we have reported the detailed fabrication process for an Y_2O_3-based memristive crossbar array architecture with its highly stable resistive switching response. Further, a non-linear analytical model is also proposed, which is capable of simulating the resistive switching response of the fabricated crossbar array. Moreover, the developed analytical model shows various characteristics such as synaptic plasticity with learning behavior, the potentiation and depression processes, and the re-stimulation mechanism. These are essential properties for neuromorphic computation application. The developed analytical model also captures the new forgetting and retention functionality, including the memory transition between STM and LTM. Therefore, the described model can be further used in the design and modeling of memristive systems for in-memory computation, neuromorphic computation and artificial neural network applications.

Data availability statement

All data that support the findings of this study are included within the article (and any supplementary files).

Acknowledgments

Sanjay Kumar would like to thank DST for providing the DST-INSPIRE (Inspire code: IF170791) PhD fellowship. The authors are grateful for the use of the DIBS facility at the Sophisticated Instrumentation Centre (SIC), IIT Indore. This work is partly supported by CSIR (No. 22(0841)/20/EMR-II).

ORCID iDs

Sanjay Kumar https://orcid.org/0000-0001-5382-2006
Shaibal Mukherjee https://orcid.org/0000-0002-9879-7278

References

[1] Naous R, AlShedivat M, Neftci E, Cauwenberghs G and Salama K N 2016 Memristor-based neural networks: synaptic versus neuronal stochasticity *AIP Adv.* **6** 111304
[2] Thomas A 2013 Memristor-based neural networks *J. Phys. D: Appl. Phys.* **46** 093001

[3] Citri A and Malenka R C 2008 Synaptic plasticity: multiple forms, functions, and mechanisms *Neuropsychopharmacol. Rev.* **33** 18–41
[4] Chang T, Jo S-H, Kim K-H, Sheridan P, Gaba S and Lu W 2011 Synaptic behaviors and modeling of a metal oxide memristive device *Appl. Phys.* A **102** 857–63
[5] Jo S H, Chang T, Ebong I, Bhadviya B, Mazumder P and Lu W 2010 Nanoscale memristor device as synapse in neuromorphic systems *Nano Lett.* **10** 1297–301
[6] Kim S, Lim M, Kim Y, Kim H-D and Choi S-J 2018 Impact of synaptic device variations on pattern recognition accuracy in a hardware neural network *Sci. Rep.* **8** 2638
[7] Hwang H-G, Woo J-U, Lee T-H, Park S-M, Lee T-G, Lee W-H and Nahm S 2020 Synaptic plasticity and preliminary-spike-enhanced plasticity in a CMOS compatible Ta_2O_5 memristor *Mater. Des.* **187** 108400
[8] Covi E, Brivio S, Serb A, Prodromakis T, Fanciulli M and Spiga S 2016 HfO_2-based memristors for neuromorphic applications *IEEE Int. Symp. On Circuits and Systems* (*ISCAS*) vol 16226481 pp 393–6
[9] Chang T 2012 Tungsten oxide memristive devices for neuromorphic applications *PhD Thesis* University of Michigan
[10] Snider G S 2008 Cortical computing with memristive nanodevices *SciDAC Rev.* **10** 58–65
[11] Jo S H, Kim K-H and Lu W 2009 High-density crossbar arrays based on a Si memristive system *Nano Lett.* **9** 870–4
[12] Tan T, Du Y, Cao A, Sun Y, Zhang H and Zha G 2018 Resistive switching of the HfO_x/HfO_2 bilayer heterostructure and its transmission characteristics as a synapse *RSC Adv.* **8** 41884–91
[13] Wu Q, Wang H, Luo Q, Banerjee W, Cao J, Zhang X, Wu F, Liu Q, Li L and Liu M 2018 Full imitation of synaptic metaplasticity based on memristor devices *Nanoscale* **10** 5875–81
[14] Chen L, Zhou W, Li C and Huang J 2021 Forgetting memristors and memristor bridge synapses with long-and short-term memories *Neurocomputing* **456** 126–35
[15] Chen L, Li C, Huang T, Chen Y, Wen S and Qi J 2013 A memristor model with forgetting effect *Phys. Lett.* A **377** 3260–5
[16] Das M, Kumar A, Kumar S, Mandal B, Khan M A and Mukherjee S 2018 Effect of surface variations on the performance of yttria based memristive system *IEEE Electron Devices Lett.* **39** 1852–5
[17] Das M, Kumar A, Singh R, Htay M T and Mukherjee S 2018 Realization of synaptic learning and memory functions in Y_2O_3 based memristive device fabricated by dual ion beam sputtering *Nanotechnology* **29** 055203
[18] Kumar S, Agrawal R, Das M, Jyoti K, Kumar P and Mukherjee S 2021 Analytical model for memristive systems for neuromorphic computation *J. Phys. D: Appl. Phys.* **54** 355101
[19] Prodromakis T, Peh B P, Papavassiliou C and Toumazou C 2011 A versatile memristor model with nonlinear dopant kinetics *IEEE Trans. Electron Devices* **58** 3099–105
[20] Khan M A, Kumar P, Das M, Htay M T, Agarwal A and Mukherjee S 2020 Drain current optimization in DIBS-grown MgZnO/CdZnO HFET *IEEE Trans. Electron Devices* **67** 2276–81
[21] Das M, Kumar A, Kumar S, Mandal B, Siddharth G, Kumar P, Htay M T and Mukherjee S 2020 Impact of interfacial SiO_2 on dual ion beam sputtered Y_2O_3-based memristive system *IEEE Trans. Nanotechnol.* **19** 153134
[22] Sharma P, Singh R, Awasthi V, Pandey S K, Garg V and Mukherjee S 2015 Detection of a high photoresponse at zero bias from a highly conducting ZnO:Ga based UV photodetector *RSC Adv.* **5** 85523
[23] Kumar S, Agrawal R, Das M, Kumar P and Mukherjee S 2020 Analytical modeling of Y_2O_3-based memristive system for synaptic applications *J. Phys. D: Appl. Phys.* **53** 305101
[24] Yang J J, Pickett M D, Li X, Ohlberg D A A, Stewart D R and Williams R S 2008 Memristive switching mechanism for metal/oxide/metal nanodevices *Nat. Nanotechnol.* **3** 429–33
[25] Yakopcic C, Taha T M, Subramanyam G, Pino R E and Rogers S 2011 A memristor device model *IEEE Electron Device Lett.* **32** 1436–8
[26] Das M, Kumar A, Mandal B, Htay M T and Mukherjee S 2018 Impact of Schottky junctions in the transformation of switching modes in amorphous Y_2O_3-based memristive system *J. Phys. D: Appl. Phys.* **51** 315102
[27] Chua L and Yang L 1988 Cellular neural networks: theory *IEEE Trans. Circuits Syst.* **35** 1257–72
[28] Chua L 2011 Resistance switching memories are memristors *Appl. Phys.* A **102** 765–83
[29] Sassine G, Barbera S L, Najjari N, Minvielle M, Dubourdieu C and Alibart F 2016 Interfacial versus filamentary resistive switching in TiO_2 and HfO_2 devices *J. Vacuum Sci. Technol. B* **34** 012202
[30] Waser R, Dittmann R, Staikov G and Szot K 2009 Redox-based resistive switching memories-nanoionic mechanisms, prospects, and challenges *Adv. Mater.* **21** 2632–63
[31] Sun W, Gao B, Chi M, Xia Q, Yang J J, Qian H and Wu H 2019 Understanding memristive switching via *in situ* characterization and device modeling *Nat. Commun.* **10** 3453
[32] Nikam R D, Kwak M and Hwang H 2021 All-solid-state oxygen ion electrochemical random-access memory for neuromorphic computing *Adv. Electron. Mater.* **7** 2100142
[33] Kim S *et al* 2019 Metal-oxide based, CMOS-compatible ECRAM for deep learning accelerator *2019 IEEE Int. Electron Devices Meeting* (*IEDM*) pp 35.7.1–35.7.4
[34] Li Y *et al* 2020 Filament-free bulk resistive memory enables deterministic analogue switching *Adv. Mater.* **32** 2003984
[35] Lee J, Nikam R D, Kwak M, Kwak H, Kim S and Hwang H 2021 Improvement of synaptic properties in oxygen-based synaptic transistors due to the accelerated ion migration in sub-stoichiometric channels *Adv. Electron. Mater.* **7** 2100219
[36] Chang T, Jo S-H and Lu W 2011 Short-term memory to long-term memory transition in a nanoscale memristor *ACS Nano* **5** 7669–76
[37] Wang Z Q, Xu H Y, Li X H, Yu H, Liu Y C and Zhu X J 2012 Synaptic learning and memory functions achieved using oxygen ion migration/diffusion in an amorphous InGaZnO memristor *Adv. Funct. Mater.* **22** 2759–65
[38] Seo K *et al* 2011 Analog memory and spike-timing-dependent plasticity characteristics of a nanoscale titanium oxide bilayer resistive switching device *Nanotechnology* **22** 254023
[39] Nikam R D, Kwak M, Lee J, Rajput K G, Banerjee W and Hwang H 2019 Near ideal synaptic functionalities in Li ion synaptic transistor using $Li_3PO_xSe_x$ electrolyte with high ionic conductivity *Sci. Rep.* **9** 18883
[40] Fuller E J, Gabaly F E, Leonard F, Agarwal S, Plimpton S J, Gedrim R B J, James C D, Marinella M J and Talin A A 2016 Li-ion synaptic transistor for low power analog computing *Adv. Mater.* **29** 1604310
[41] Xiao T P, Bennett C H, Feinberg B, Agarwal S and Marinella M J 2020 Analog architectures for neural network acceleration based on non-volatile memory *Phys. Rev.* **7** 031301
[42] Nikam R D, Lee J, Choi W, Banerjee W, Kwak M, Yadav M and Hwang H 2021 Ionic sieving through one-atom-thick 2D material enables analog nonvolatile memory for neuromorphic computing *Small* **17** 1–11